Featured Article

Efficient Elimination of B-Lineage Lymphomas by Anti-CD20–Auristatin Conjugates

Che-Leung Law, Charles G. Cerveny, Kristine A. Gordon, Kerry Klussman, Bruce J. Mixan, Dana F. Chace, Damon L. Meyer, Svetlana O. Doronina, Clay B. Siegall, Joseph A. Francisco, Peter D. Senter, and Alan F. Wahl

Seattle Genetics, Inc., Bothell, Washington

ABSTRACT

The anti-CD20 antibody rituximab is useful in the treatment of certain B-cell malignancies, most notably non-Hodgkin's lymphoma. Its efficacy has been increased when used in combination with chemotherapy, yet anti-CD20 monoclonal antibodies (mAbs) directly conjugated with drugs such as doxorubicin (Dox) have failed to deliver drug or to demonstrate antitumor activity. We have produced anti-CD20 antibody-drug conjugates that possess potent antitumor activity by using the anti-mitotic agent, monomethyl auristatin E (MMAE), linked via the lysosomally cleavable dipeptide, valine-citrulline (vc). Two anti-CD20 conjugates, rituximab-vcMMAE and 1F5-vcMMAE, were selectively cytotoxic against $CD20^+$ B-lymphoma cell lines, with IC_{50} values ranging from 50 ng/mL to 1 μg/mL. Unlike rituximab, which showed diffuse surface localization, rituximab-vcMMAE capped and was internalized within 4 hours after binding to $CD20^+$ B cells. Internalization of rituximab-vcMMAE was followed by rapid G_2-M phase arrest and onset of apoptosis. Anti-CD20 antibody-drug conjugates prepared with Dox were internalized and localized as with rituximab-vcMMAE, yet these were not effective for drug delivery (IC_{50} > 50 μg/mL). Consistent with *in vitro* activity, rituximab-vcMMAE showed antitumor efficacy in xenograft models of CD20-positive lymphoma at doses where rituximab or rituximab-Dox conjugates were ineffective. These data indicate that anti-CD20–based antibody-drug conjugates are effective antitumor agents when prepared with a stable, enzyme-cleavable peptide linkage to highly potent cytotoxic agents such as MMAE.

Received 5/25/04; revised 8/30/04; accepted 9/2/04.

The costs of publication of this article were defrayed in part by the payment of page charges. This article must therefore be hereby marked *advertisement* in accordance with 18 U.S.C. Section 1734 solely to indicate this fact.

Requests for reprints: Alan F. Wahl, Seattle Genetics, Inc., 21823–30th Drive Southeast, Bothell, WA 98021. Phone: (425) 527-4610; Fax: (425) 527-4609; E-mail: awahl@seagen.com.

INTRODUCTION

More than 270,000 people in the United Stated suffer from non-Hodgkin's lymphoma. In 2001, an estimated 56,200 new cases were diagnosed, and 26,300 United States deaths were attributed to the disease (American Cancer Society Facts and Figures, 2001). Non-Hodgkin's lymphoma is frequently treated with conventional chemotherapies, such as cyclophosphamide, fludarabine, or chlorambucil, or combination therapies, such as cyclophosphamide, vincristine, and prednisolone or cyclophosphamide, doxorubicin (Dox), vincristine, and prednisolone (1). Increasingly, treatment includes rituximab (Rituxan), a chimeric monoclonal antibody (mAb) targeting the CD20 cell surface antigen. Rituximab affects antitumor activity primarily via apoptosis induction (2), complement-mediated cytotoxicity (3–5), and antibody-dependent cell-mediated cytotoxicity (6–8). Rituximab was approved by the Food and Drug Administration for treatment of relapsed or refractory follicular lymphoma (9). Patients treated with weekly infusions of rituximab showed a 48% response rate (6% complete responses, 42% partial responses; ref. 10), with a median response duration of about 12 months (11, 12).

The efficacy of anti-CD20 mAbs has been improved in two ways. First, two anti-CD20 radioisotope conjugates approved for clinical use (13–15) offer improved efficacy over unmodified forms of anti-CD20 (16) yet are difficult to produce, are unstable, and may be associated with undesirable myelosuppression (17). Secondly, efficacy can be improved by combination with standard cytotoxic therapies (18). In intermediate-grade non-Hodgkin's lymphoma, rituximab in combination with cyclophosphamide, Dox, vincristine, and prednisolone chemotherapy increased complete response rate from 60 to 75% and prolonged 1-year event-free survival from 49 to 69% and increased overall survival from 68 to 83% as compared with cyclophosphamide, Dox, vincristine, and prednisolone alone (19). Despite advances, a significant number of patients relapse or are refractive to these interventions.

An effective approach to enhancing the antitumor activity of mAbs is linkage to cytotoxic drugs or toxins. Antibody-drug conjugates can deliver cell-killing agents to cells via mAbs provided they internalize upon antigen binding. Gemtuzumab ozogamicin (Mylotarg, Wyeth, Collegeville, PA), an anti-CD33 mAb-calicheamicin conjugate for treating refractory acute promyelocytic leukemia, was the first Food and Drug Administration-approved antibody-drug conjugate (20). Antibody-drug conjugates of anti-CD20 have been evaluated and generally found to be ineffective. Anti-CD20 Dox conjugates (21), and more recently a rituximab-liposomal Dox (22) and anti-CD20-ricin A-chain conjugate, were not effective against CD20 positive cells (23). These results were partially attributed to differences in CD20 trafficking because other conjugates could induce modulation and internalization of mAb/antigen com-

plexes, whereas a comparable effect was not observed with anti-CD20 (24).

CD20 undergoes receptor recycling (25), and after surface binding, the anti-CD20 mAb 1F5 accumulated proximal to Golgi apparatus in lymphoma cells (25). It was thus unknown whether more potent drugs or those with different mechanism of action or mAb linkage chemistry could produce an effective anti-CD20–based antibody-drug conjugate. We constructed two anti-CD20–antibody-drug conjugates incorporating auristatin E-based cytotoxics via peptide linkage. The auristatins are synthetic antimitotic agents related to the marine natural product dolastatin 10 and ~200 times more potent than Dox (26). They act by inhibiting polymerization of tubulin and hence prevent formation of the mitotic apparatus (27). A dipeptide linkage cleavable by lysosomal proteases within antigen-positive cells has recently been applied to link auristatin E-based drugs to mAbs (26). This novel drug linkage applied to anti-CD30 mAbs produced antibody-drug conjugates with potent and highly selective activity against CD30-positve tumors (28), prompting its application to anti-CD20 mAbs. Two anti-CD20 mAbs, rituximab and 1F5, were conjugated to monomethyl auristatin E (MMAE) through a cathepsin B-cleavable valine-citrulline (vc) dipeptide linkage. We report here that anti-CD20 mAbs coupled via lysosomally cleavable linkers to the highly potent cytotoxic drug MMAE effectively and specifically kill CD20-positive tumor cells *in vitro* and have significant antitumor activity in xenograft models of non-Hodgkin's lymphoma.

MATERIALS AND METHODS

Cells and Reagents. Rituximab (chimeric anti-CD20 Rituxan, IDEC Pharmaceuticals, San Diego, CA, and Genentech, Inc., South San Francisco, CA) was obtained from RX USA (Jamaica, NY). mAb 1F5, an IgG2a against CD20 was reported previously (29). The hybridoma was grown in RPMI 1640 (Life Technologies, Inc., Gaithersburg, MD) supplemented with 10% fetal bovine serum (complete medium). Antibody was purified from culture supernatants by protein A chromatography. Ramos, Raji, and Daudi Burkitt's lymphoma cell lines were from American Type Culture Collection (Manassas, VA), and the ALCL line, Karpas 299 was from the DSMZ (Braunschweig, Germany). All cell lines used were determined mycoplamsa free by PCR. Goat antimouse IgG FITC and goat antihuman IgG FITC were from Jackson Immunoresearch (West Grove, PA).

Drug Synthesis. The synthesis of MMAE and the activated vc linker used in both the auristatin and Dox syntheses was as described previously (26). The synthesis of Dox with the vc linker has been described previously (30).

Antibody-Drug Conjugate Preparation. Antibody-drug conjugates were prepared as described previously (26, 28). Briefly, the antibody interchain disulfides were first reduced with excess dithiothreitol. Resulting hinge-region thiols were alkylated with drug-linker (vcMMAE or vcDox) in 10% molar excess. Reactions were quenched with excess cysteine, purified by desalting over Sephadex G25 resin, sterile filtered, and stored frozen.

The concentration of antibody-drug conjugates was determined by UV absorbance. The drug/Ab ratios were determined either by UV absorbance (Dox conjugates) or by determining the number of residual thiols with 5,5′-dithiobis(2-nitrobenzoic acid) (MMAE conjugates). The degree of aggregation, determined by size exclusion chromatography, for all antibody-drug conjugates used in this study was <3%. The level of free drug in all antibody-drug conjugate, determined by reverse phase high-performance liquid chromatography, was <1%. Drug/mAb ratios for both chimeric and murine antibody-drug conjugate preparations ranged from 7.0 to 7.5 for the vcMMAE conjugates and 6.0 to 6.5 for the Dox conjugates.

Flow Cytometry. To evaluate CD20 expression on cell lines, 1×10^6 cells were combined with 10 μg/mL rituximab in ice-cold PBS (staining medium) for 30 minutes on ice, and washed twice with ice cold staining media to remove unbound mAb. Cells were stained with secondary goat antihuman IgG-FITC, at saturation (10 μg/mL) in ice-cold staining medium, incubated 30 minutes on ice, and washed as above. Labeled cells were examined by flow cytometry on a Becton Dickinson FACScan flow cytometer gated to exclude nonviable cells and analyzed using Winlist 4.0 software (Verity Software House, Topsham, ME). Background-corrected mean fluorescence intensity was determined for each cell type.

To evaluate cell binding of mAb and antibody-drug conjugate, 1×10^6 Raji cells were combined with serial dilutions of mAb 1F5, rituximab, or their antibody-drug conjugates in ice-cold staining media for 30 minutes on ice and washed twice with ice-cold staining medium. Cells were then incubated with goat anti-mouse IgG FITC (for 1F5 and 1F5 antibody-drug conjugate) or goat anti-human IgG FITC (for rituximab or rituximab–antibody-drug conjugate) at 10 μg/mL on ice for 30 minutes and washed as described above. Labeled cells were analyzed by flow cytometry as above.

CD20 Expression Level. Quantitation of cell surface CD20 was determined with DAKO QiFiKiT flow cytometric indirect immunofluorescence assay (DAKO A/S, Glostrup, Denmark).

Growth Inhibition Assays. Cytotoxicity was measured by Alamar Blue (Biosource International, Camarillo, CA) dye reduction assay (31). Briefly, Alamar Blue (40%) in complete media was freshly prepared before assay. After 92 hours of drug exposure, Alamar Blue solution was added to cells to 10% culture volume. Cells were incubated for 4 hours, and dye reduction was measured on a Fusion HT fluorescent plate reader (Packard Instruments, Meriden, CT) with excitation at 540 nm and emission at 590 nm. IC_{50} was defined as the concentration resulting in a 50% reduction in growth or viability as compared with untreated control cultures.

Growth Arrest and Apoptosis. Apoptosis and cell death were assessed by Annexin V binding to the cell surface and propidium iodide (PI) exclusion with the Annexin V-FITC Apoptosis Detection kit (BD PharMingen, San Diego, CA). Annexin V binds phosphotidyl serine displayed on the outer cell membrane during the onset of apoptosis (32) and staining with the DNA intercalating dye PI, normally excluded from viable cells indicates loss of membrane integrity in dead or dying cells (33). For analysis of cell cycle position after drug exposure, cells were cultured in complete medium and agent and at the indicated times labeled with bromodeoxyuridine (10 μmol/L final; Sigma, St. Louis, MO) for 20 minutes. Nascent DNA synthesis was detected with anti-bromodeoxyuridine (BD Bio-

sciences, San Jose, CA), total DNA content was detected with PI, and analysis for cell cycle position and apoptosis was conducted by flow cytometry on a FACScan as described previously (34).

Microscopy for mAb/Antibody-Drug Conjugate Trafficking. Ramos cells suspended at 5×10^5 cells per mL were treated with rituximab, rituximab-vcMMAE, or rituximab-vc-Dox at 5 μg/mL in complete medium. After a 4-hour incubation at 37°C with 5% CO_2, the cells were washed once in 1× PBS (pH 7.4) to remove unbound antibodies. Cells were fixed and permeabilized with paraformaldehyde/saponin as provided in the Cytofix/Cytoperm kit (BD Biosciences) and then stained with antibodies according to manufacturer's instruction. Rituximab and rituximab antibody-drug conjugates were detected with an Alexa Fluor-568 conjugated mouse antihuman IgG (H+L) antibody with minimal cross-reactivity to mouse IgG (Molecular Probes, Eugene, OR). Subcellular compartments were visualized with mouse antibodies raised against clathrin heavy chain, caveolin-1, GM130, or Lamp-1/CD107a, (BD Biosciences), followed by an Alexa Fluor-488–conjugated goat antimouse IgG (H+L) antibody with minimal cross-reactivity to human IgG (Molecular Probes). After washes, nuclei were stained by resuspending cells in PBS containing 1 μg/mL 4′,6-diamidino-2-phenylindole (Roche, Basel, Switzerland). Cells were mounted on poly-D-lysine–coated cover glass in a DABCO antifade medium containing 25 mg/mL 1,4-diazobicyclo-(2,2,2)-octane (Sigma) in a solution of 90% spectrophotometric grade glycerol and 10% 1× PBS (35). Fluorescence images were acquired with a Leitz Orthoplan epi-fluorescence microscope fitted with a Nikon 990 digital camera.

***In vivo* Antitumor Activities of Anti-CD20 Antibody-Drug Conjugates.** Localized and disseminated xenograft models of human B-lymphoma were used to evaluate the efficacy of anti-CD20 antibody-drug conjugates. To model localized lymphoma, 5×10^6 Ramos Burkitt's lymphoma cells were implanted s.c. into the right flank of C.B.-17 SCID mice (Harlan, Indianapolis, IN). Therapy was initiated when the mean tumor size in each group of five animals was ~100 mm^3. Treatment consisted of i.v. injections of mAb or antibody-drug conjugate every 4 days for three injections. Tumor size was determined using the formula $(L \times W^2)/2$. To model disseminated disease, 5×10^6 Ramos cells in 200 μL of PBS per mouse were injected i.v. into the tail veins of female C.B.-17 SCID mice. Therapy was started on day 9 after tumor cell injection. Treatment consisted of i.v. injections of mAb or antibody-drug conjugate into the tail veins every 4 days for three injections. Animals were observed for the development of hind limb paralysis; at that point, they were euthanized. Survival of animals posttumor injection was recorded. Kaplan-Meier statistical analysis was based on time to tumor quadrupling for the solid tumor model and differences in survival time for the disseminated disease model. All animal studies were conducted in accordance with Animal Care and Use Committee Guidelines.

RESULTS

Preparation of Anti-CD20 Antibody-Drug Conjugates. MMAE was prepared by replacing a protected form of monomethylvaline for valine in the synthesis of auristatin E (26). MMAE was then additionally modified with maleimidocaproyl-vc to result in vcMMAE, which contained a *p*-aminobenzylcarbamate spacer between the MMAE and the linker. Similarly, Dox was modified to result in vcDox containing a *p*-aminobenzylcarbamate spacer between Dox and the linker (30). The resulting structures of drug derivatives used in these studies are shown appended to mAb-SH in Fig. 1. Four antibody-drug conjugates, rituximab-vcMMAE, rituximab-vcDox, 1F5-vcMMAE, and an irrelevant IgG-vcMMAE, were synthesized to the drug/mAb ratios specified in Materials and Methods for this study.

The vc linkage exhibits high stability in blood and efficient release of fully active drug in the presence of human lysosomal cathepsin B (26). Subsequent to proteolytic cleavage, residual linker between the peptide and the drug undergoes fragmentation, leading to release of fully active MMAE (26) or Dox (30).

Cell Characterization and Sensitivity to Unconjugated Drugs. Human B-cell lymphoma lines, Daudi, Raji, and Ramos, and the ALCL line, Karpas 299, were evaluated by flow cytometry to assess their relative CD20 expression levels with rituximab followed by a goat anti-human IgG-FITC reagent. Background corrected mean fluorescence intensities for Daudi, Ramos, and Raji cells were 880, 400, and 650 units, respectively (Table 2). The ALCL line Karpas 299, used as an antigen-negative control, showed a mean fluorescence intensity of 3.5 units. Estimation of CD20 density on these cells was determined with a Dako QiFiKiT indirect immunofluorescence flow cytometric assay (36). Using this, the density of CD20 were determined to be 3.7×10^5, 4.1×10^5, and 4.5×10^5 copies per cell for Ramos, Raji, and Daudi lines, respectively (Table 2). The negative control cell line Karpas 299 showed no signal above background with this method.

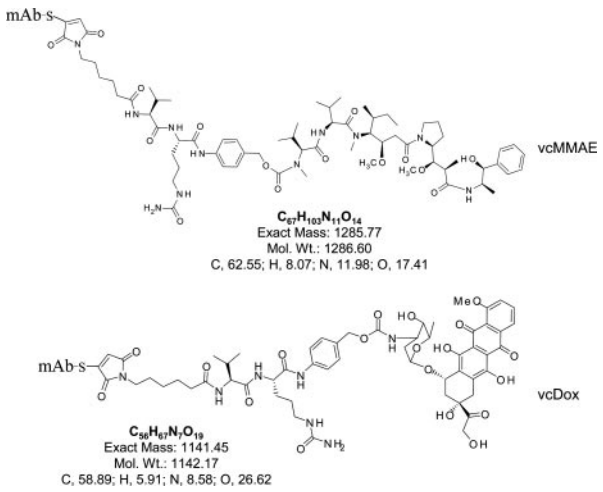

Fig. 1 Structures of linker-drug systems used for mAb conjugation. The structures of vcMMAE and vcDox appended to mAb salfhydryl groups are depicted. Antibody-drug conjugates were prepared by controlled partial reduction of internal mAb disulfides with dithiothreitol, followed by addition of the linker drugs as described in Materials and Methods. Stable thioether-linked antibody-drug conjugates were formed upon addition of the free sulfhydryl groups on the mAbs to maleimides present on the drugs.

Binding of Anti-CD20 and Anti-CD20 Antibody-Drug Conjugates to CD20$^+$ B Cells. To evaluate the binding characteristics of rituximab and corresponding antibody-drug conjugates, Raji cells were combined with increasing concentrations of either mAb or antibody-drug conjugates, incubated on ice to block antigen modulation, and washed to remove unbound material. Goat antihuman IgG-FITC was used to detect mAb or antibody-drug conjugate for rituximab and an irrelevant, isotype-matched chimeric IgG, whereas a goat antimouse IgG FITC for was used to detect the murine mAb 1F5 as described in Materials and Methods. Fig. 2 shows fluorescence intensity *versus* concentration for cells stained with rituximab alone or antibody-drug conjugates of Dox or MMAE. Conjugation of rituximab or either Dox or MMAE had minimal effect on the binding when compared with the parental, unconjugated mAb. Binding of Dox-containing antibody-drug conjugates was slightly more attenuated than that with MMAE (Fig. 2). Similar results were obtained with mAb 1F5 and respective antibody-drug conjugate of 1F5 (data not shown).

Cell Sensitivity to Unconjugated Drugs and Anti-CD20 Antibody-Drug Conjugates. Tumor cells were evaluated for sensitivity to free Dox and MMAE by exposing cells for 2 hours, followed by replating in fresh media and incubation for an additional 96 hours. At 4 hours before harvest, cells were incubated with Alamar Blue, a reducible dye that provides readout of cell viability (31). Table 1 shows the drug sensitivities in IC_{50} values of Daudi, Ramos, Raji, and Karpas 299 cells. MMAE IC_{50} values ranged from 48 to 300 times more potent than Dox against these cell lines. To evaluate the potency and selectivity of various antibody-drug conjugates, cells were incubated for 2 hours, washed to remove unbound antibody-drug conjugate, replated in fresh media, and incubated as above for cell viability assessment. Results from one representative experiment are shown in Fig. 3*A*. Rituximab-vcMMAE was highly cytotoxic to Ramos cells with resultant IC_{50} of 45 ng/mL. Neither rituximab-vcDox nor an irrelevant IgG-vcMMAE were

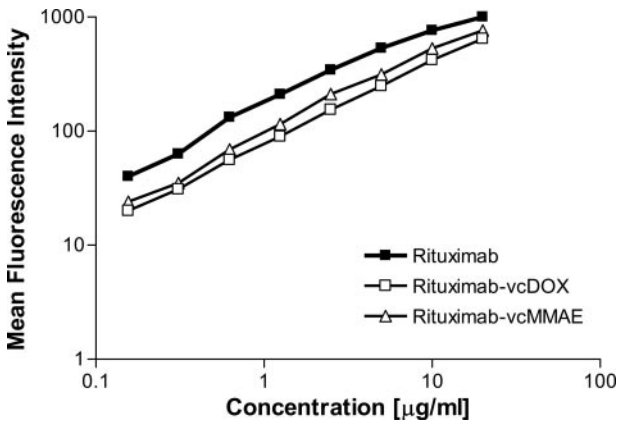

Fig. 2 Comparitive mAb and antibody-drug conjugates binding to CD20-positive cells. Increasing concentrations of rituximab or rituximab-vcMMAE or rituximab-vcDox were combined with Raji cells, incubated on ice to prevent antigen modulation, and washed. The bound mAb or antibody-drug conjugates were stained with excess goat antihuman IgG-FITC, and the resultant cell-bound complex was detected by flow cytometry.

Table 1 Sensitivity of cells to unconjugated drugs

Cell line	MMAE IC_{50}*	Dox IC_{50}	Activity ratio MMAE/Dox †
Daudi (CD20+)	4.6 ± 4.3	225 ± 35	49
Ramos (CD20+)	1.5 ± 0.7	300 ± 140	200
Raji (CD20+)	4.0 ± 0.7	190 ± 13	48
Karpas 299 (CD20-)	3.2 ± 1.4	975 ± 50	300

* IC_{50} values are in nmol/L and are expressed as the mean and SD of at least three independent experimental titrations, each performed in quadruplicate.

† Activity ratio is calculated by IC_{50Dox}/IC_{50MMAE}.

growth inhibitory to these cells at the highest levels tested (50 μg/mL). Similar, albeit not as potent, results were obtained with the mAb 1F5-vcMMAE against CD20-positive lines Daudi, Ramos, and Raji (Table 2). 1F5-vcDox antibody-drug conjugate was not effective (data not shown). CD20-negative Karpas 299 cells were not sensitive to any antibody-drug conjugate up to the maximum level tested (50 μg/mL; Table 2). To additionally demonstrate the selectivity and stability of the antibody-drug conjugate, cells were continuously exposed to rituximab-vcMMAE for 96 hours (Fig. 3*B*). Continuous exposure of CD20-positive Ramos cells to rituximab-vcMMAE produced in an IC_{50} of 8 ± 2 ng/mL, whereas the IC_{50} for CD20-negative Karpas 299 cells treated in parallel remained >5000 ng/mL (Fig. 3*B*). IC_{50} values for each antibody-drug conjugate determined from at least three independent experiments and the relative expression of CD20 on these cells are summarized in Table 2. Thus, treatment with anti-CD20-vcMMAE resulted in antigen-dependent cytotoxicity not seen with the unmodified mAb alone or anti-CD20-vcDox.

Induction of Apoptosis by Rituximab-vcMMAE. To assess the mechanism of toxicity, Ramos cells were incubated with a high level (5 μg/mL) of rituximab, rituximab-vcMMAE, and rituximab-vcDox. At 1, 4, and 24 hours after exposure, cells were removed from cultures, and the degree of apoptosis and cell death were determined by surface Annexin V binding and loss of PI exclusion, respectively (33). The percentages of apoptotic cells (determined as Annexin V^+/PI^- events) and dead cells (Annexin V^+/PI^+ events) in cultures treated with rituximab, rituximab-vcMMAE, or rituximab-vcDox ranged from 1 to 5% apoptotic/3 to 5% dead at 1 or 4 hours post-treatment and were indistinguishable from untreated cells by these criteria (data not shown). At 24 hours post-exposure, values were unchanged for untreated cells or cells treated with rituximab or rituximab-vcDox (Fig. 4*A*). In contrast, cells treated with rituximab-vcMMAE were increased to 19% apoptotic and 60% dead.

To examine the cell cycle effects and apoptosis induced by rituximab antibody-drug conjugates, Ramos cells cultured under the conditions described above were labeled at 2, 8, and 24 hours posttreatment with bromodeoxyuridine for 20 minutes to detect nascent DNA synthesis and with PI to detect total DNA content and analyzed by flow cytometry. Dox appended to other internalizing mAbs can produce a potent G_2 arrest in antigen-positive cells (37). However, treatment with rituximab or rituximab-vcDox at 5 μg/mL showed no significant perturbation in cell cycle position or DNA fragmentation compared with untreated control cells, suggesting the free drug was not delivered

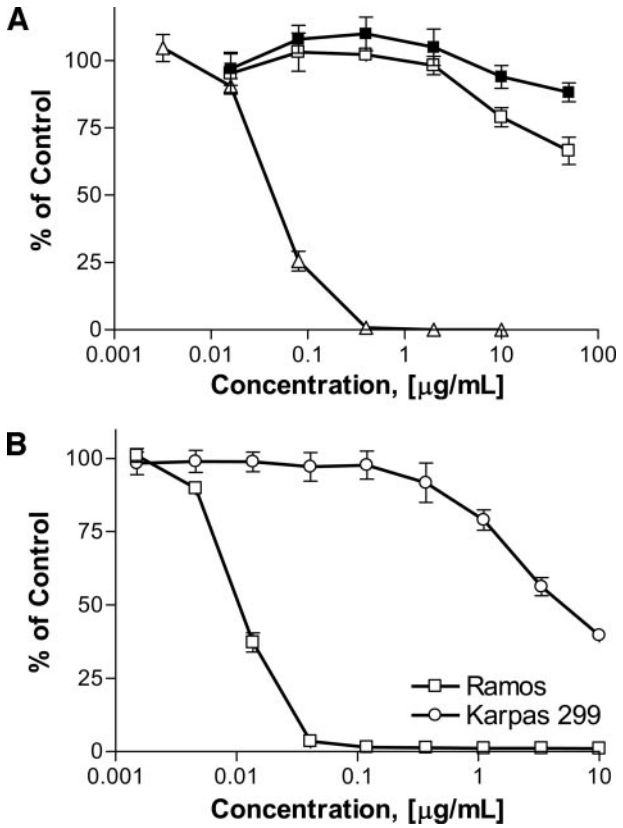

Fig. 3 Sensitivity of cells to antibody-drug conjugates. Cells in complete media were incubated with titrations of mAb or antibody-drug conjugates for 2 hours to allow binding, washed to remove unbound reagent, replated in fresh complete media, and returned to incubation for an additional 94 hours. Alamar blue was added to culture wells 4 hours before evaluation. Cell viability was assessed by detecting dye metabolism on a fluorescence plate reader and compared with that of control wells cultured in the presence of complete media alone. *A*, representative dose-response curves of Ramos cells to rituximab (■), rituximab-vcDox (□), rituximab-vcMMAE (△). *B*. To additionally evaluate antibody-drug conjugate stability and selectivity, CD20-positive Ramos (□) and CD20-negative Karpas 299 cells (○) were continuously exposed to a titration of rituximab-vcMMAE for 96 hours before viability determination. Data points are the mean of quadruplicate determinations (± SDs).

to the cell interior. In contrast, cells exposed to rituximab-vcMMAE showed significant loss of G_1 DNA content and increase in G_2 DNA content within 8 hours of exposure, the effects being consistent with a rapid G_2-M phase arrest induced by MMAE (Fig. 4*B*). The G_1 population reached its nadir within 8 hours of exposure, and G_2 population increased from 8% in untreated pools to 50% at 12 hours after rituximab-vcMMAE exposure (data not shown). At 24 hours post-exposure, S-phase cells were undetectable, and the discrete G_2 population became highly diffuse with sub-G_2 and sub-G_1 DNA content consistent with apoptotic DNA fragmentation (Fig. 4*B*). These data suggest active MMAE was rapidly released and affected growth inhibition within 8 hours of exposure. Growth arrest and apoptotic cell death were not seen after exposure to equivalent concentrations of rituximab or rituximab-vcDox. Parallel studies done with an irrelevant IgG-vcMMAE showed cell cycle and apoptotic signatures indistinguishable from untreated (control) cells (data not shown).

Internalization of Rituximab Antibody-Drug Conjugates. Cell cycle effects suggested rituxan-vcMMAE delivered active MMAE to the cell interior within 8 hours of exposure (Fig. 4). To evaluate cell surface modulation of rituximab and its antibody-drug conjugates, Ramos cells were incubated for 20 minutes at 4°C with saturating levels (10 μg/mL) of either the mAb alone, rituximab-vcMMAE, or rituximab-vcDox. Cells were washed at 4°C to remove unbound material and either maintained on ice in the presence of NaN_3 to block modulation or shifted to 37°C. At progressive time points, cells were stained with goat antihuman IgG-FITC and analyzed by flow cytometry to detect the level of remaining surface mAb or antibody-drug conjugate. Fig. 5*A* shows nominal change in surface levels of either rituximab or the two antibody-drug conjugate on cells kept at 4°C for the course of the 120 minutes study. Similarly, surface loading with rituximab remained relatively constant during this time on cells shifted to 37°C. In contrast, surface levels of rituximab-vcMMAE or rituximab-vcDox declined significantly in cells shifted to 37°C over the course of the assay. Within 2 hours, >50% and >70% of rituximab-vcMMAE and rituximab-vcDox, respectively, was lost from the cell surface, suggesting that antibody-drug conjugate was either shed from the surface to the media or preferentially internalized by the cells. Whereas saturation binding of antibody-drug conjugates are comparable with parent mAb (Fig. 2) and because CD20 is not known to be shed by B cells (11,

Table 2 Sensitivity of cells to anti-CD20 drug conjugates

Cell line	Rituximab-vcMMAE IC_{50} (μg/mL) *,†	Rituximab-vcDox IC_{50} (μg/mL)	1F5-vcMMAE IC_{50} (μg/mL)	IgG-vcMMAE ‡ IC_{50} (μg/mL)	Flow cytometry results	
					MFI §	CD20 density (copies/10^5 cells)
Daudi	1.04 ± 0.75	>50	1.27 + 0.87	>50	880	4.5×10^5
Ramos	0.04 ± 0.002	>50	0.15 + 0.008	>50	400	3.7×10^5
Raji	1.5 ± 0.31	>50	3.9 + 0.3	>50	650	4.1×10^5
Karpas 299	>50	>50	>50	>50	3.5	0

* IC_{50} values are the mean and SE of at least three independent experimental titrations, each performed in quadruplicate.

† One μg/mL rituximab-vcMMAE carries 47.0 nmol/L of the drug-linker component vcMMAE, 1 μg/mL rituximab-vcDox carries 41.5 nmol/L vcDox.

‡ Nonbinding, rituximab–isotype-matched IgG.

§ Mean fluorescence intensity (MFI) of cells stained with rituximab and a secondary (goat antihuman IgG)-FITC conjugate.

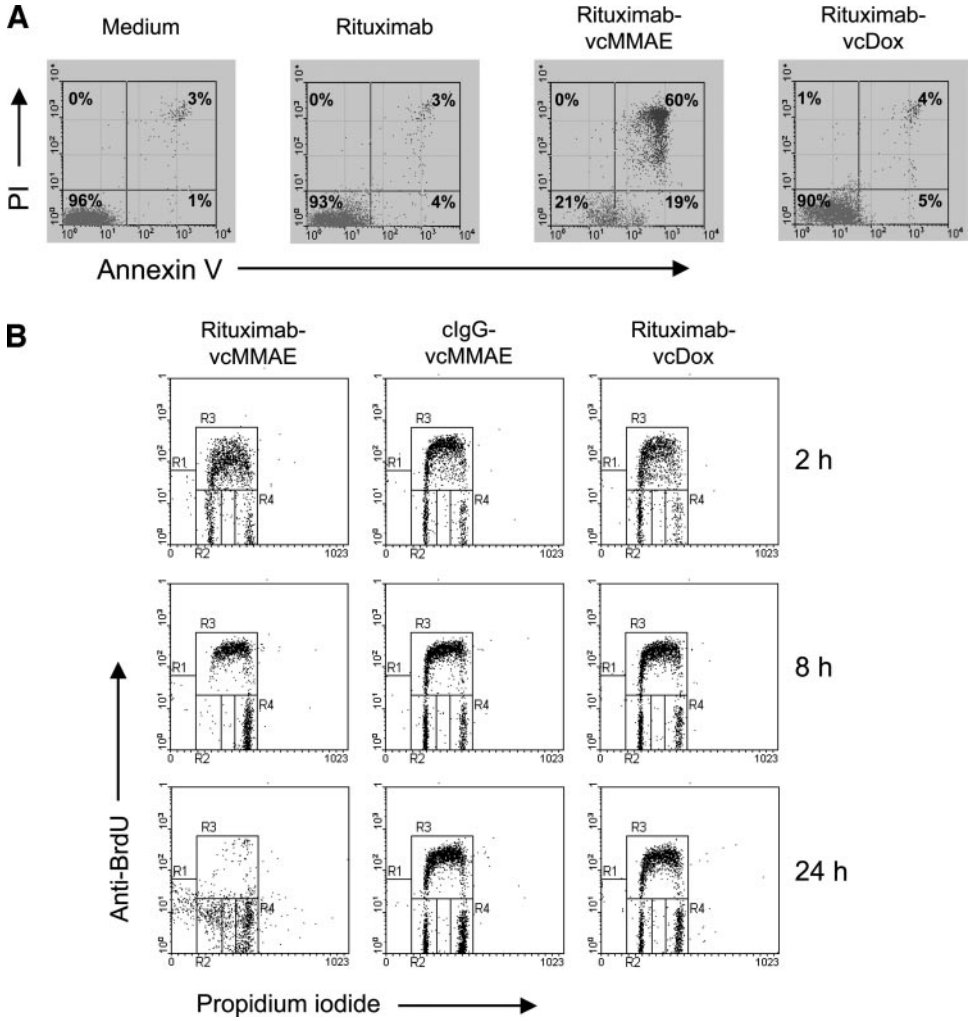

Fig. 4 Selective induction of G_2 growth arrest and apoptosis. *A*. Ramos cells were incubated with medium alone, 5 μg/mL rituximab, rituximab-vcMMAE, or rituximab-vcDox. At 24 hours after exposure, cells were removed from cultures and stained with Annexin V-FITC and PI. The range of apoptotic cells (Annexin V^+/PI^-) and of dead cells (Annexin V^+/PI^+) was determined by flow cytometric analysis of each population. *B*. Cells were treated as in *A* for the specified duration and allowed to incorporate bromodeoxyuridine (BrdUrd) into DNA for 20 minutes before harvest. At harvest, cells were fixed/permeabilized and stained with anti-BrdUrd–FITC to detect nascent DNA synthesis and stained with PI for total DNA content at the indicated times post-antibody–drug conjugate exposure. Gates R2, R3, and R4 designate the positions of G_1, S phase, and G_2-M phase populations, respectively. Gate R1 designates cells of less than G_1 DNA content (apoptotic).

38), the decline in surface bound rituximab-vcMMAE and rituximab-vcDox at 37°C as shown in Fig. 5*A* suggested an increased internalization of the antibody-drug conjugate-CD20 complexes.

To track trafficking and localization, Ramos cells were incubated with rituximab or antibody-drug conjugates for 4 hours at 37°C, fixed, and permeabilized to allow indirect fluorescence microscopy for the cellular localization. mAb and antibody-drug conjugates were detected with fluorochrome-labeled mouse antihuman IgG (H+L) as described in Material and Methods. Antibodies against the lysosomal marker Lamp-1/CD107a (39) and the Golgi marker GM130 (40) were used to examine potential co-localization of rituximab and/or rituximab antibody-drug conjugates to these organelles. The possibility that mAb or antibody-drug conjugates were endocytosed via clathrin-coated pits or lipid raft pathways was addressed with antibodies against the clathrin heavy chain or caveolin-1, respectively. Microscopic localization of fluorescence signals in representative cells are shown in Fig. 5, *B–D*. Cells treated with rituximab showed predominantly diffuse surface staining (Fig. 5*B*, left column). Signals were well segregated from those of clathrin, caveolin-1, GM130, and Lamp-1 (Fig. 5*B*, center and right columns), suggesting minimal internalization of the rituximab-CD20 complexes. In contrast, cells incubated with rituximab-vcMMAE showed extensive patching and capping of the antibody-drug conjugate–CD20 complexes (Fig. 5*C*, left column), and intracellular staining of the rituximab-vcMMAE-CD20 complexes was apparent at this 4-hour time point. The antibody-drug conjugate–CD20 complexes co-localized with Lamp-1, the clathrin heavy chain, and caveolin-1 but not with GM130 (Fig. 5*C*, center and right columns), suggesting that rituximab-vcMMAE might be internalized via clathrin- and/or caveolin-mediated endocytosis and trafficked to the lysosomal compartment. Similarly, rituximab-vcDox also appeared to be internalized and trafficked to the lysosomal compartment (Fig. 5*D*). Neither binding nor internalization of the mAb or antibody-drug conjugates could be detected on CD20-negative Karpas 299 cells (data not shown).

***In vivo* Efficacy of Rituximab-vcMMAE against B-Lymphoma Xenografts.** To examine the therapeutic potential of anti-CD20 drug conjugates, the *in vivo* activity of rituximab-vcMMAE was evaluated in localized and dissemi-

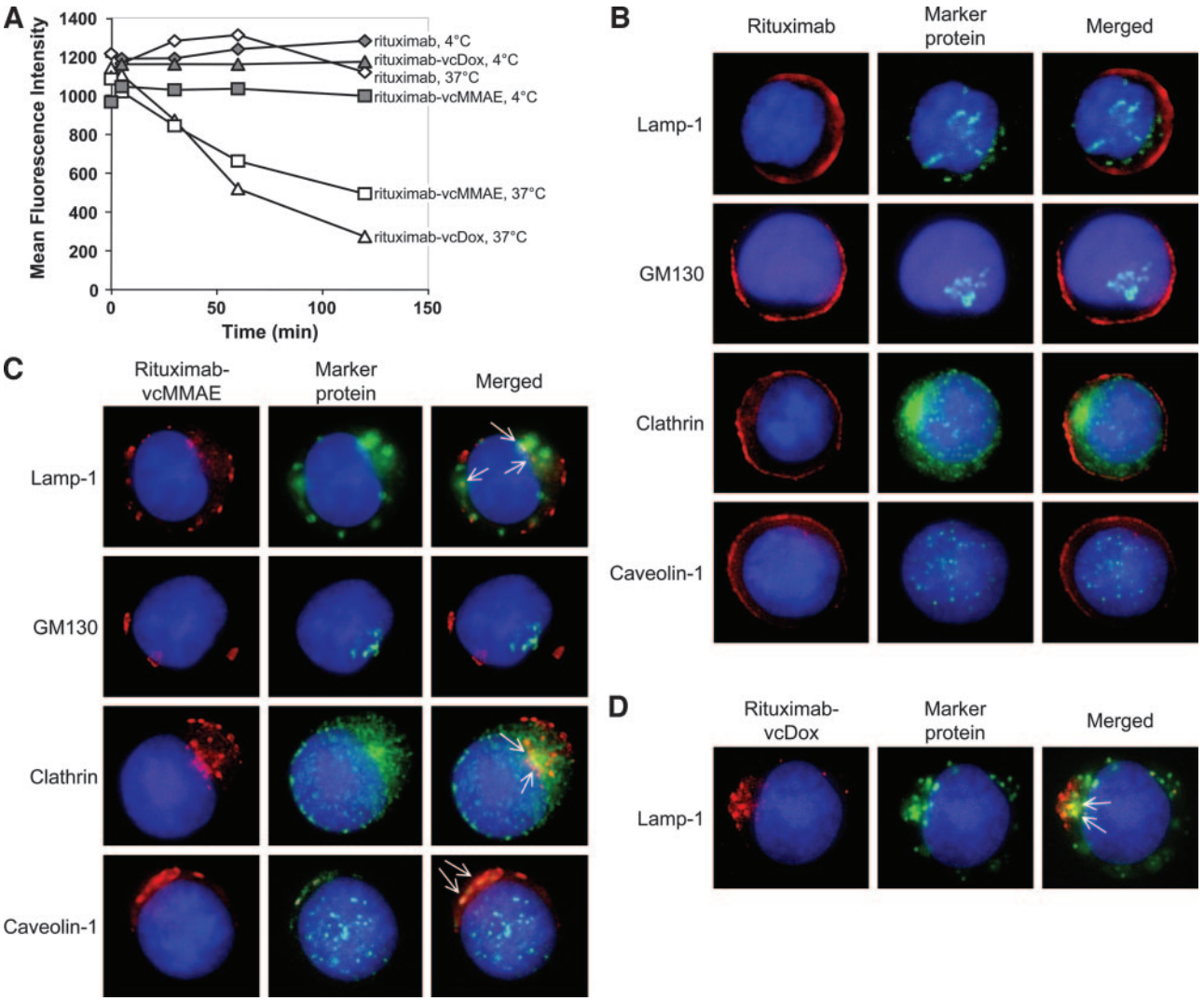

Fig. 5 Trafficking and cellular localization of rituximab and rituximab–antibody-drug conjugates. *A*. Ramos B cells were treated with saturating concentrations of rituximab, rituximab-vcMMAE, or rituximab-vcDox in complete medium at 4°C for 30 minutes. Unbound antibody or antibody-drug conjugates were removed by washing cells in medium. Cells were incubated at either 4°C with NaN_3 or 37°C. At the indicated time points, a portion of the cells was removed from each culture, and cell surface-bound rituximab or rituximab antibody-drug conjugates was detected by flow cytometry with goat anti-human IgG FITC. *B*. Ramos B cells were treated with rituximab in complete medium at 37°C for 4 hours. Cells were fixed and permeabilized by paraformaldehyde/saponin and cell-associated rituximab and marker proteins lysosome associated membrane protein 1 (LAMP-1), Golgi-associated protein 130 (GM130), clathrin, and caveolin-1 were detected with respective fluorochrome-conjugated secondary antibodies. Nuclei were stained with 4′,6-diamidino-2-phenylindole as described in Materials and Methods. Shown are representative single cell images. The *left column* shows the rituximab signals, the *center column* shows the indicated marker protein signals, and the *right column* shows the merged images. *C*. Localization of rituximab-vcMMAE and marker proteins was determined as described in *B*. *Arrows* indicate co-localization of rituximab-vcMMAE with lysosomes (Lamp-1), clatherin, and caveolae membranes (caveolin-1). *D*. Localization of rituximab-vcDox and Lamp-1 was determined as described in *B*. *Arrows* indicate co-localization of rituximab-vcDox with Lamp-1.

nated tumor models of Ramos lymphoma cells in SCID mice. Relatively stringent conditions in which treatment was delayed until tumors were well established in mice for >1 week were used to differentiate the *in vivo* efficacies of mAb and antibody-drug conjugates. In a localized tumor model, SCID mice were implanted s.c. with 5×10^6 Ramos cells into the right flank. The tumor size in each group of five animals was allowed to progress to a mean size of 100 mm^3, ~11 days after implantation (Fig. 6*A*), before therapy was initiated. Treatment consisted of i.v. injections of mAb or antibody-drug conjugate every 4 days for three injections with 1 (data not shown) and 3 mg/kg/injection. Tumors in the untreated, rituximab, rituximab-vcDox, control nonbinding cIgG-vcMMAE, or rituximab-vcMMAE at 1 mg/kg (data not shown) groups grew rapidly and reached an average of >800 mm^3 by day 20. Animals treated with the maximum-tolerated dose of Dox (3 mg/kg) also showed no significant reduction in the rate of tumor progression compared with untreated animals (data not shown). Free MMAE admin-

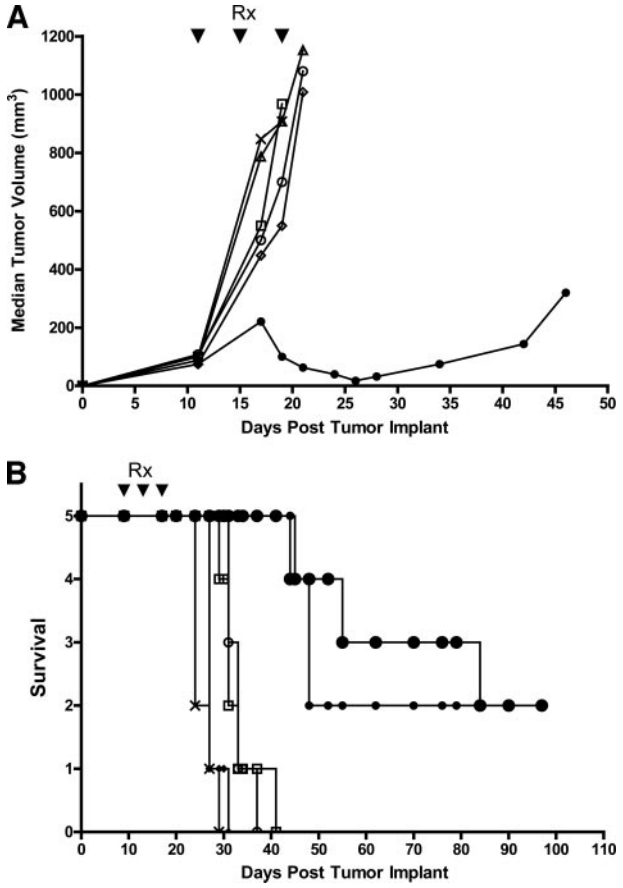

Fig. 6 Efficacy of rituximab–antibody-drug conjugate in B-cell lymphoma models. (A) Antitumor activity of rituximab and rituximab antibody-drug conjugates were evaluated in treating a model of s.c. Ramos lymphoma in SCID mice. Mice were implanted with 5×10^6 Ramos B-lymphoma cells into the right flank. Mice (five/group) were either left untreated or received rituximab, rituximab-vcMMAE, rituximab-vcDox or an irrelevant IgG-vcMMAE on a schedule of q4dx3 starting when the tumor size in each group of 5 animals averaged 100 mm^3 (11 days posttumor implantation). Free MMAE was administered at a dose equivalent to that carried by the ADC. Rituximab-vcMMAE treated animals showed significant differences in tumor volume quadrupling compared with other groups ($P = 0.0027$) (B) To model disseminated lymphoma, SCID mice were injected through the tail vein with 5×10^6 Ramos lymphoma cells. Tumors were allowed to establish and then treated with rituximab-vcMMAE or controls at 3 and 6 mg/kg starting on day 9 posttumor injection. Rituximab-vcMMAE treated animals showed significant survival advantage compared with untreated control groups ($P = 0.0019$).

istered at 0.12 mg/kg (~100 nmol/kg or the molar equivalent of MMAE present in 3 mg/kg rituximab-vcMMAE) had no impact on tumor growth. In contrast, rituximab-vcMMAE at 3 mg/kg was able to significantly delay tumor growth ($P = 0.0027$ compared with untreated control group; Fig. 6*A*). In a model of disseminated B-cell lymphoma in SCID mice, disease was induced by i.v. injection of 5×10^6 Ramos cells. Treatment with mAb, antibody-drug conjugates, or free MMAE was delayed for 9 days after tumor implantation. Survival in the untreated group or groups receiving either rituximab or control cIgG-vcMMAE at 6 mg/kg or the molar equivalent of free drug sharply declined 20 days after tumor implantation (Fig. 6B), and no surviving animals remained in these groups 40 days posttumor injection. In contrast, survival in the group treated with 6 mg/kg rituximab-vcMMAE was 60% on day 55 posttumor injection and remained at 40% at the close of study on day 100. Similarly, survival in the group treated with 3 mg/kg rituximab-vcMMAE was 40% on day 45 posttumor injection, which was maintained for an additional 45 days. These selective and statistically significant results ($P = 0.0019$) correlated well with *in vitro* data. No overt toxicity was observed in animals treated with the therapeutic doses of mAb or antibody-drug conjugates described above. We have previously shown that a similarly constructed cIgG-vcMMAE was well tolerated at 30 mg/kg and determined the maximum-tolerated dose to be ~40 mg/kg (28).

DISCUSSION

Anti-CD20 mAbs can initiate B-cell lymphoma killing through multiple mechanisms, including apoptosis (2), complement-mediated lysis (3–5), and FcR-mediated antibody-dependent cell-mediated cytotoxicity and phagocytosis (6, 7). Efficacy has been improved by conjugation to radionuclides, as with Zevalin (13, 41) and Bexxar (17), or in combination with cytotoxic therapies (18). However, these improvements are not curative, and resistance or relapse after treatment remains significant in CD20-positive disease. Anti-CD20 mAbs linked to cytotoxics (21), plant toxins (23), or to immunoliposomes containing Dox (22) were ineffectual avenues for drug delivery to the cell interior. Surprisingly, anti-CD20 conjugated to the antimitotic MMAE has showed significant antitumor activity. CD20 is displayed at moderate levels, 0.2 to 4×10^5 copies/cell on malignant B cells (24), and is internalized and redistributed to the surface by the process of receptor-mediated endocytosis (42). This modulation is altered by anti-CD20 binding (24, 42), resulting in CD20 redistribution into rafts or membrane compartments on the cell surface (43, 44).

Rituximab alone is weakly proapoptotic (6%) on Ramos B cells at 10 μg/mL, the activity nominally enhanced by mAb homodimers (45). Rituximab-vcMMAE selectively induced apoptosis, with IC_{50} of 40 ng/mL on Ramos cells (Fig. 3). Target cells growth arrested in G_2-M phase within 8 hours and were apoptotic within 24 hours of exposure to rituximab-vcMMAE (Fig. 4), suggesting efficient internalization and drug release. The MMAE-related dolastatin 10 and auristatin PE induce growth arrest and apoptosis by interference with microtubule assembly (27) and the cytotoxicity of rituximab-vcMMAE is likely related.

Nonbinding antibody-drug conjugates showed little effect on cell cycle or toxicity after 4 days of exposure, indicating high linkage stability and drug attenuation outside the cell (Figs. 3 and 4*B*). The lysosomally cleaved vc linker offers a significant stability advantage over acid-cleaved linkers (26, 30). CD20 modulation may occur slowly compared with other internalizing antigens such as CD33; thus, successful drug delivery via CD20 may require a stable, highly potent antibody-drug conjugate and stable cell surface binding. Cytotoxicity observed with both rituximab-vcMMAE and mAb 1F5-vcMMAE (Table 2) indicate the drug delivery is not limited to a specific mAb. Ramos cells, expressing the least CD20 of the three positive lines examined

(3.7×10^5 copies/cell), are the most sensitive to the antibody-drug conjugate (Table 1), suggesting that expression, receptor internalization, trafficking, and drug release are important variables to antibody-drug conjugate potency. The avidity and internalization of 1F5 antibody-drug conjugate may be differ compared with rituximab-vcMMAE or the peptide linkage in the former may be less accessible to proteolysis and drug release than rituximab-vcMMAE.

Both -vcDox and -vcMMAE antibody-drug conjugates were modulated from the cell surface at increased rates compared with rituximab alone (Fig. 5), and both -vcDox and the -vcMMAE antibody-drug conjugates capped and subsequently co-localized with lysosomal Lamp-1 protein. CD20 is associated with caveolin-rich lipid rafts (43, 44), yet the antibody-drug conjugate might redirect CD20 molecules to clathrin-coated pits or more efficient trafficking to the lysosome; thus, both clathrin- and/or caveolin-associated endocytosis are potential pathways for antibody-drug conjugate to enter the lysosome. The effects of the dipeptide linker (Fig. 1) on patching, capping, and internalization of antibody-drug conjugate is being evaluated.

Interestingly, trafficking of rituximab-vcDox to the lysosomal compartment did not result in cytotoxicity. Although IC_{50} of the free drugs differ by ~200-fold (Table 2), the IC_{50} for the respective antibody-drug conjugate differ by >1000-fold (Table 2), suggesting a delivery advantage of MMAE-based antibody-drug conjugates. At 7.5 vcMMAE molecules per mAb molecule, the amount of free drug delivered by antibody-drug conjugate to Ramos cells at their IC_{50} (40 ng/mL rituximab-vcMMAE) is 2 nmol/L. This is in close agreement with the IC_{50} of free MMAE (1.5 nmol/L) and suggests efficient drug delivery. In contrast, the highest concentration of rituximab-vcDox tested (50 μg/mL) could potentially deliver 2 μmol/L Dox. This is ~5-fold higher than the IC_{50} value (300 nmol/L) of free Dox, yet the antibody-drug conjugate was nominally cytotoxic to Ramos cells. Dox released from rituximab-vcDox might become trapped in the acidic environment of the lysosomes (46), attenuating the activity of rituximab-vcDox, or may require proteosome-mediated transport to the nucleus for maximum effect (47). Alternatively, given the role of tubulin in intracellular vesicular transport, the potential exists for tubulin-disrupting agents such as MMAE to alter trafficking upon entry into the cytoplasm (48, 49).

Rituximab-vcMMAE was efficacious in two stringent xenograft models of CD20-positive lymphoma. Rituximab alone has *in vivo* antitumor activity if co-administered with the lymphoma cell implant and dosed at ≥10 mg/kg (6). However, treatment of established tumors with rituximab administered at 10 mg/kg showed only marginal antitumor activity (22, 50). Shown herein, 3 or 6 mg/kg rituximab alone were not effective against established tumors, whereas equivalent doses of rituximab-vcMMAE showed significant antitumor activity and survival advantage for the hosts (Fig. 6). No drug-related toxicities were noted at these levels. We have previously treated mice with up to 30 mg/kg IgG-vcMMAE (26, 28) with no overt toxicities. Single-dose maximum-tolerated dose for IgG-vcMMAE was determined to be 40 mg/kg (28). Toxicity does not appear to be cumulative because 12 consecutive doses of IgG-vcMMAE administered to mice at 10 mg/kg produced no detectable side effects (51). Taken together, these suggest that a considerable therapeutic window may exist for anti-CD20-vcMMAE. The limited number of CD20-positive cell lines tested here suggests that antibody-drug conjugates of anti-CD20-vcMMAE are effective against tumor lines displaying this marker.

The highly potent and stable drug linker system vcMMAE, coupled with anti-CD20 mAbs such as rituximab and 1F5, may comprise an effective new cytotoxic drug delivery system, providing a new tool with which to efficiently target CD20-positive disease. It will be of great interest to determine whether this drug/linkage technology could expand the therapeutic potentials of other tumor-selective mAbs that do not efficiently internalize upon antigen binding. Additional CD20-positive cell lines and animal models will better establish the significance of these findings and their potential for the treatment of rituximab-resistant $CD20^+$ lymphomas.

REFERENCES

1. Al Ismail SA, Whittaker JA, Gough J. Combination chemotherapy including epirubicin for the management of non-Hodgkin's lymphoma. Eur J Cancer Clin Oncol 1987;23:1379–84.

2. van der Kolk LE, Evers LM, Omene C, et al. CD20-induced B cell death can bypass mitochondria and caspase activation. Leukemia (Baltimore) 2002;16:1735–44.

3. Harjunpaa A, Junnikkala S, Meri S. Rituximab (anti-CD20) therapy of B-cell lymphomas: direct complement killing is superior to cellular effector mechanisms. Scand J Immunol 2000;51:634–41.

4. Bellosillo B, Villamor N, Lopez-Guillermo A, et al. Complement-mediated cell death induced by rituximab in B-cell lymphoproliferative disorders is mediated in vitro by a caspase-independent mechanism involving the generation of reactive oxygen species. Blood 2001;98:2771–7.

5. Kennedy AD, Solga MD, Schuman TA, et al. An anti-C3b(i) mAb enhances complement activation, C3b(i) deposition, and killing of CD20+ cells by rituximab. Blood 2003;101:1071–9.

6. Clynes RA, Towers TL, Presta LG, Ravetch JV. Inhibitory Fc receptors modulate in vivo cytoxicity against tumor targets. Nat Med 2000;6:443–6.

7. Selenko N, Maidic O, Draxier S, et al. CD20 antibody (C2B8)-induced apoptosis of lymphoma cells promotes phagocytosis by dendritic cells and cross-priming of CD8+ cytotoxic T cells. Leukemia (Baltimore) 2001;15:1619–26.

8. Cartron G, Dacheux L, Salles G, et al. Therapeutic activity of humanized anti-CD20 monoclonal antibody and polymorphism in IgG Fc receptor FcgammaRIIIa gene. Blood 2002;99:754–8.

9. Leget GA, Czuczman MS. Use of rituximab, the new FDA-approved antibody. Curr Opin Oncol 1998;10:548–51.

10. Grillo-Lopez AJ, White CA, Varns C, et al. Overview of the clinical development of rituximab: first monoclonal antibody approved for the treatment of lymphoma. Semin Oncol 26(S14):66–73, 1999.

11. McLaughlin P, Grillo-Lopez AJ, Link BK, et al. Rituximab chimeric anti-CD20 monoclonal antibody therapy for relapsed indolent lymphoma: half of patients respond to a four-dose treatment program. J Clin Oncol 1998;16:2825–33.

12. Carter P. Improving the efficacy of antibody-based cancer therapies. Nat Rev Cancer 2001;1:118–29.

13. Grillo-Lopez AJ. Zevalin: the first radioimmunotherapy approved for the treatment of lymphoma. Expert Rev Anticancer Ther 2002;2:485–93.

14. Zelenetz AD. A clinical and scientific overview of tositumomab and iodine I 131 tositumomab. Semin Oncol 30(S4):S22–30, 2003.

15. Kaminski MS, Zelenetz AD, Press OW, et al. Pivotal study of iodine I 131 tositumomab for chemotherapy-refractory low-grade or transformed low-grade B-cell non-Hodgkin's lymphomas. J Clin Oncol 2001;19:3918–28.

16. Witzig TE. Radioimmunotherapy for patients with relapsed B-cell non-Hodgkin lymphoma. Cancer Chemother Pharmacol 2001;48(S1): S91–95.

17. Witzig TE, Gordon LI, Cabanillas F, et al. Randomized controlled trial of yttrium-90-labeled ibritumomab tiuxetan radioimmunotherapy versus rituximab immunotherapy for patients with relapsed or refractory low-grade, follicular, or transformed B-cell non-Hodgkin's lymphoma J Clin Oncol 2002;20:2453–63.

18. Coiffier B. Rituximab in combination with CHOP improves survival in elderly patients with aggressive non-Hodgkin's lymphoma. Semin Oncol 2002;29:18–22.

19. Grillo-Lopez AJ, White CA, Dallaire BK, et al. Rituximab: the first monoclonal antibody approved for the treatment of lymphoma. Curr Pharm Biotechnol 2000;1:1–9.

20. Sievers EL, Linenberger M. Mylotarg: antibody-targeted chemotherapy comes of age. Curr Opin Oncol 2001;13:522–7.

21. Braslawsky GR, Kadow K, Knipe J, et al. Adriamycin(hydrazone)-antibody conjugates require internalization and intracellular acid hydrolysis for antitumor activity. Cancer Immunol Immunother 1991;33: 367–74.

22. Sapra P, Allen TM. Internalizing antibodies are necessary for improved therapeutic efficacy of antibody-targeted liposomal drugs. Cancer Res 2002;62:7190–4.

23. Goulet AC, Goldmacher VS, Lambert JM, Baron C, Roy DC, Kouassi E. Conjugation of blocked ricin to an anti-CD19 monoclonal antibody increases antibody-induced cell calcium mobilization and CD19 internalization. Blood 1997;90:2364–75.

24. Vervoordeldonk SF, Merle PA, van Leeuwen EF, dem Borne AE, Slaper-Cortenbach IC. Preclinical studies with radiolabeled monoclonal antibodies for treatment of patients with B-cell malignancies. Cancer (Phila.) 1994;73:1006–11.

25. Michel RB, Mattes MJ. Intracellular accumulation of the anti-CD20 antibody 1F5 in B-lymphoma cells. Clin Cancer Res 2002;8:2701–13.

26. Doronina SO, Toki BE, Torgov MY, et al. Development of potent monoclonal antibody auristatin conjugates for cancer therapy. Nat Biotechnol 2003;21:778–84.

27. Pettit GR. The dolastatins. Fortschr Chem Org Naturst 1997; 70:1–79.

28. Francisco JA, Cerveny CG, Meyer DL, et al. cAC10-vcMMAE, an anti-CD30-monomethyl auristatin E conjugate with potent and selective antitumor activity. Blood 2003;102:1458–65.

29. Press OW, Appelbaum F, Ledbetter JA, et al. Monoclonal antibody 1F5 (anti-CD20) serotherapy of human B cell lymphomas. Blood 1987; 69:584–91.

30. Dubowchik GM, Firestone RA. Cathepsin B-sensitive dipeptide prodrugs. 1. A model study of structural requirements for efficient release of doxorubicin. Bioorg Med Chem Lett 1998;8:3341–6.

31. Nakayama GR, Caton MC, Nova MP, Parandoosh Z. Assessment of the Alamar Blue assay for cellular growth and viability in vitro. J Immunol Methods 1997;204:205–8.

32. Martin SJ, Reutelingsperger CP, McGahon AJ, et al. Early redistribution of plasma membrane phosphatidylserine is a general feature of apoptosis regardless of the initiating stimulus: inhibition by overexpression of Bcl-2 and Abl. J Exp Med 1995;182:1545–56.

33. Vermes I, Haanen C, Steffens-Nakken H, Reutelingsperger C. A novel assay for apoptosis. Flow cytometric detection of phosphatidylserine expression on early apoptotic cells using fluorescein labelled Annexin V. J Immunol Methods 1995;184:39–51.

34. Donaldson KL, McShea A, Wahl AF. Separation by counterflow centrifugal elutriation and analysis of T- and B-lymphocytic cell lines in progressive stages of cell division cycle. J Immunol Methods 1997;203: 25–33.

35. Johnson GD, Davidson RS, McNamee KC, Russell G, Goodwin D, Holborow EJ. Fading of immunofluorescence during microscopy: a study of the phenomenon and its remedy. J Immunol Methods 1982;55: 231–42.

36. Poncelet P, Carayon P. Cytofluorometric quantification of cell-surface antigens by indirect immunofluorescence using monoclonal antibodies. J Immunol Methods 1985;85:65–74.

37. Wahl AF, Donaldson KL, Mixan BJ, Trail PA, Siegall CB. Selective tumor sensitization to taxanes with the mAb-drug conjugate cBR96-doxorubicin. Int J Cancer 2001;93:590–600.

38. Kunala S, Macklis RM. Ionizing radiation induces CD20 surface expression on human B cells. Int J Cancer 2001;96:178–81.

39. Fukuda M. Lysosomal membrane glycoproteins. Structure, biosynthesis, and intracellular trafficking. J Biol Chem 1991;266:21327–30.

40. Nakamura N, Rabouille C, Watson R, et al. Characterization of a cis-Golgi matrix protein, GM130. J Cell Biol 1995;131:1715–26.

41. Grillo-Lopez AJ. Monoclonal antibody therapy for B-cell lymphoma. Int J Hematol 2002;76:385–93.

42. Pulczynski S, Boesen AM, Jensen OM. Modulation and intracellular transport of CD20 and CD21 antigens induced by B1 and B2 monoclonal antibodies in RAJI and JOK-1 cells: an immunofluorescence and immunoelectron microscopy study. Leuk Res 1994;18: 541–52.

43. Deans JP, Robbins SM, Polyak MJ, Savage JA. Rapid redistribution of CD20 to a low density detergent-insoluble membrane compartment. J Biol Chem 1998;273(1):344–8.

44. Semac I, Palomba C, Kulangara K, et al. Anti-CD20 therapeutic antibody rituximab modifies the functional organization of rafts/ microdomains of B lymphoma cells. Cancer Res 2003;63:534–40.

45. Ghetie MA, Bright H, Vitetta ES. Homodimers but not monomers of Rituxan (chimeric anti-CD20) induce apoptosis in human B-lymphoma cells and synergize with a chemotherapeutic agent and an immunotoxin. Blood 2001;97:1392–8.

46. Gong Y, Duvvuri M, Krise JP. Separate roles for the Golgi apparatus and lysosomes in the sequestration of drugs in the multidrug-resistant human leukemic cell line HL-60. J Biol Chem 2003;278: 50234–9.

47. Kiyomiya K, Matsuo S, Kurebe M. Mechanism of specific nuclear transport of adriamycin: the mode of nuclear translocation of adriamycin-proteasome complex. Cancer Res 2001;61:2467–71.

48. Hamm-Alvarez SF, Alayof BE, Himmel HM, et al. Coordinate depression of bradykinin receptor recycling and microtubule-dependent transport by Taxol. Proc Natl Acad Sci USA 1994;91:7812–16.

49. Scott CD, Baxter RC. Regulation of soluble insulin-like growth factor-II/mannose 6-phosphate receptor in hepatocytes from intact and regenerating rat liver. Endocrinology 1996;137:3864–70.

50. Ma D, McDevitt MR, Barendswaard E, et al. Radioimmunotherapy for model B cell malignancies using 90Y-labeled anti-CD19 and anti-CD20 monoclonal antibodies. Leukemia (Baltimore) 2002;16:60–6.

51. Afar DE, Bhaskar V, Ibsen E, et al. Preclinical validation of anti-TMEFF2-auristatin E-conjugated antibodies in the treatment of prostate cancer. Mol Cancer Ther 2004;3:921–32.

Clinical Cancer Research

Efficient Elimination of B-Lineage Lymphomas by Anti-CD20–Auristatin Conjugates

Che-Leung Law, Charles G. Cerveny, Kristine A. Gordon, et al.

Clin Cancer Res 2004;10:7842-7851.